Magnetospheric line radiation: 6.5 years of observations by the DEMETER spacecraft

B Bezdeková, F Němec, Michel Parrot, O Santolík, O Kruparova

RESEARCH ARTICLE

Key Points:
- Survey of 1230 MLR events identified in the DEMETER spacecraft data
- Event occurrence compared with geomagnetic activity and solar wind parameters
- Energy-latitude plots of electron flux variations related to the MLR occurrence derived

Correspondence to:
B. Bezděková,
baja@etranslator.biz

Magnetospheric line radiation: 6.5 years of observations by the DEMETER spacecraft

B. Bezděková[1], F. Němec[1], M. Parrot[2], O. Santolík[1,3], and O. Kruparova[3]

[1]Faculty of Mathematics and Physics, Charles University in Prague, Prague, Czech Republic, [2]LPC2E/CNRS, Orléans, France, [3]Institute of Atmospheric Physics, The Czech Academy of Sciences, Prague, Czech Republic

Abstract Frequency-time spectrograms of electromagnetic waves observed in the inner magnetosphere in the frequency range of about 1–8 kHz are sometimes formed by several nearly horizontal and almost equidistant intense lines. Such events are called magnetospheric line radiation (MLR). We use a list of 1230 MLR events identified in all the data measured by the low-altitude satellite Detection of Electro-Magnetic Emissions Transmitted from Earthquake Regions (DEMETER) during the duration of the mission (2004–2010). We compare the occurrence of MLR events with solar wind parameters and geomagnetic indices using a superposed epoch analysis. It is found that MLR events occur more often after periods of enhanced geomagnetic activity, being statistically related to specific solar wind parameters. Moreover, the length of the analyzed time interval allows us to investigate the influence of the solar cycle and the season of the year. The events occur more often during the northern winter and spring than during the northern summer. As for the spatial distribution of the events, they occur less frequently at geomagnetic longitudes of the South Atlantic Anomaly. We analyze energy spectra of electrons precipitating in this area at the times of MLR events, and we derive energy-latitude plots of electron flux variations related to the MLR occurrence. Finally, we perform a detailed wave analysis of two MLR events for which high-resolution multicomponent data are available. The events are right-handed and nearly circularly polarized, propagating at oblique wave normal angles from larger radial distances and larger geomagnetic latitudes.

1. Introduction

Frequency-time spectrograms of electromagnetic waves at frequencies between about 1 and 8 kHz observed in the inner magnetosphere are sometimes formed by several intense spectral lines. These are nearly equidistant in frequency, and they may exhibit a rather slow, typically positive, frequency drift. Such electromagnetic wave events are called magnetospheric line radiation (MLR), and they have been reported in both ground-based data [e.g., *Rodger et al.*, 1999, 2000a, 2000b; *Manninen*, 2005] and satellite data [e.g., *Bell et al.*, 1982; *Rodger et al.*, 1995; *Parrot et al.*, 2005; *Němec et al.*, 2007a, 2009, 2012a, 2012b]. Although such events have been known already for decades, their origin is still unclear.

It was suggested that MLR events might be related to power line harmonic radiation (PLHR), i.e., wave events generated by electromagnetic radiation from electric power systems on the ground [*Bullough*, 1995]. However, *Rodger et al.* [1999] analyzed ground-based measurements of MLR events performed at Halley, Antarctica, and they found that the frequency spacing of individual lines forming the MLR events does not correspond to harmonics of electric power system frequencies, i.e., to 50 or 60 Hz. The approximately exponential form of the distribution of MLR line spacings indicates that a generation mechanism of MLR events is different than PLHR. The conclusion of MLR being a natural emission, not related to PLHR, was further confirmed by *Rodger et al.* [2000a]. Temporal properties of MLR events measured at Halley, Antarctica, were analyzed by *Rodger et al.* [2000b]. They reported that MLR events are typically observed for about 30 min, and their occurrence is sometimes connected with previous geomagnetic activity (24–48 h after very large storms, $Kp > 6$). However, no stronger dependence of MLR occurrence on the level of the geomagnetic activity has been discovered.

Rodger et al. [1995] reported the results of the first systematic survey of satellite observations of MLR events using the data measured by the International Satellites for Ionospheric Studies (ISIS) 1 and 2 spacecraft. They distinguished two different classes of events. The events of the first class are formed by spectral lines with a broadband appearance and frequency drifts of a few tens of hertz per minute. The frequency spacing of

individual lines forming these events is variable, not corresponding to the multiples of 50 or 60 Hz. Technically speaking, only these events can be considered as MLR events according to the recent classification. The events of the second class are characterized by spectral lines with very narrow bandwidths and no frequency drift. These typically lie close to harmonics of 50 or 60 Hz. More detailed analysis of the differences between these two classes of events using the data from the Detection of Electro-Magnetic Emissions Transmitted from Earthquake Regions (DEMETER) spacecraft was given by *Němec et al.* [2007a]. The second class of events is believed to be due to electromagnetic radiation from electric power systems on the ground, and these events would be nowadays classified as PLHR [see, e.g., *Němec et al.*, 2006, 2007b, 2008, 2010a].

The analysis of a large-scale MLR event observed simultaneously on board the low-altitude satellite DEMETER and on the ground (Sodankyla, Finland) was reported by *Parrot et al.* [2007]. The event was shown to last for about 2 h and to occur over a large area in the Northern Hemisphere (more than 7 million km^2). Surveys of MLR events measured by the DEMETER spacecraft were provided by *Němec et al.* [2009, 2012a]. More than 4 years of the satellite data containing a few hundreds of events were analyzed. It has been shown that the events occur more often during the day than during the night and that they occur more often during/after the periods of increased geomagnetic activity. The events occurred mostly at $L > 2$, being approximately limited to within the plasmasphere. The occurrence rate of the events was found to be lower above the South Atlantic Anomaly (SAA) than elsewhere on the globe, and a lack of energetic electrons in the drift loss cone to the east of the SAA was suggested as a possible explanation. Frequency spacing between individual lines was found to be larger during stronger geomagnetic activity (i.e., during the times of the compressed plasmasphere). There appears to be no connection between the frequency spacing or the frequency drift and the L shell where the events were observed. It was suggested that the waves might be guided by the inner plasmapause boundary.

In the present paper we show results of a systematic analysis of all MLR events identified in the DEMETER spacecraft data during its entire 6.5 year mission. This results in a larger data set as compared to previously reported studies which used a subset of the currently available data. We use this large data set to analyze the connection of MLR events with other phenomena, i.e., to identify the most favorable conditions for their occurrence. We evaluate variations of energetic electron fluxes measured by DEMETER in relation to MLR events. We also perform a detailed propagation analysis of two MLR events for which relevant high-resolution multicomponent data are available. Section 2 describes the DEMETER satellite, the identification of MLR events, and the resulting data set. The obtained results are presented in section 3, and they are discussed in section 4. Finally, the main results are summarized in section 5.

2. Data Set

We have used data from the DEMETER spacecraft, which was a French low-altitude satellite launched in June 2004. The satellite had a nearly Sun-synchronous (about 10:30 and 22:30 LT) circular orbit, and it measured data at all geomagnetic latitudes lower than 65°. The original altitude of about 710 km was decreased to 660 km in December 2005. The mission ended in December 2010. The satellite operated in two different modes, called Burst and Survey. High-resolution data were collected during the Burst mode. This mode was, however, active only above areas of a specific interest. Lower resolution Survey mode data were always acquired. In the very low frequency (VLF) range that we are interested in, power spectra of one electric and one magnetic field component were calculated on board during the Survey mode. Unfortunately, the magnetic field data suffer from a significant amount of interference between 1 and 8 kHz, so that exclusively VLF electric field data will be used in the present study. The frequency resolution is 19.53 Hz, and the time resolution is 2 s or 0.5 s, depending on the mode of the instrument. In addition to the one-component Survey mode data, all the six components of the electromagnetic field were measured at frequencies lower than about 1 kHz in the Burst mode. These can be used to perform a detailed wave analysis of MLR events. More detailed information about the DEMETER spacecraft, the electric and magnetic field measurements on board, and the related data processing were given by *Parrot* [2006], *Berthelier et al.* [2006], and *Santolík et al.* [2006a].

We started from the list of MLR events compiled by *Němec et al.* [2009] and later extended by *Němec et al.* [2012a] to contain all MLR events identified until the end of September 2008. We have expanded this list to contain all MLR events identified during the duration of the DEMETER mission, i.e., until the end of 2010. The events were visually identified in frequency-time spectrograms of power spectral density of electric field fluctuations, using the same procedure as before. A frequency-time spectrogram with a fixed frequency range from 1 to 8 kHz and a fixed power scale from 10^{-3} to $10^2 \mu V^2 m^{-2} Hz^{-1}$ was prepared for each satellite half orbit. An example of such spectrogram is shown in Figure 1, where an MLR event can be seen between about
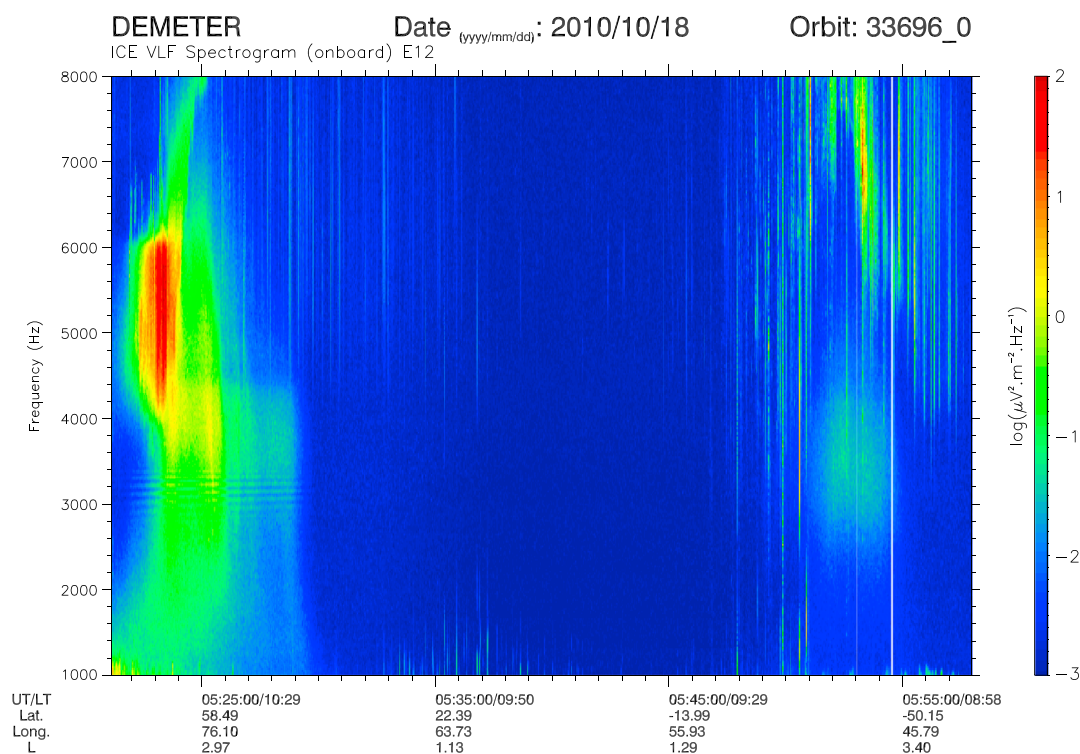
Figure 1. Example frequency-time spectrogram of power spectral density of electric field fluctuations which contains an MLR event. The event occurred between about 05:22 UT and 05:29 UT at frequencies around 3000 Hz. Several nearly horizontal lines forming the event can be clearly seen.

05:22 UT and 05:29 UT at frequencies of about 3 kHz. It is formed by several nearly horizontal lines which exhibit a slow positive frequency drift. We note that at both lower and higher frequencies the event looks like a hiss emission of a comparable intensity but without an apparent line structure.

Altogether, 1230 MLR events were identified in 1054 half orbits (out of 57,574 in total). Note that the number of half orbits with MLR events is lower than the total number of events, because in some cases two events occur during a single half orbit. As reported already by *Němec et al.* [2009], MLR events occur preferentially during daytime half orbits. Namely, 781 events were identified in diurnal half orbits, and 449 events were identified in nocturnal half orbits.

3. Results

3.1. Most Favorable Solar Wind Conditions

The large number of MLR events identified in 6.5 years of the DEMETER data allows us to statistically evaluate the influence of the solar activity on the occurrence of the events. The black curve in Figure 2a indicates the number of MLR events detected in a moving 90 day wide time interval normalized by the total number of DEMETER half orbits for which the VLF Survey mode data were available in a given time interval as a function of the central time of this interval. Note that this number does not represent the occurrence rate: it can reach values larger than 1 if we systematically observed more than one MLR event per half orbit. However, in reality, the observed average values around 0.02 mean that we observe one MLR event per 50 half orbits on average. It can be seen that the normalized number of detected MLR events is noticeably lower at the end of 2007 and at the beginning of 2008. The overplotted blue curve with the average sunspot number shows that this period precedes the solar minimum, but the overall correlation is weak. Moreover, distinct peaks of the normalized number of MLR events can be identified, generally during the northern winter or spring. Not every winter is accompanied by the peak, but, nevertheless, the MLR occurrence may depend on the season of the year. We investigate this effect more in detail in Figure 2b, which shows the monthly variation of the number of identified MLR events normalized by the total number of DEMETER half orbits for which the VLF Survey mode data were available in a given month. It can be seen that on average there are about twice as many MLR events detected during the northern winter and spring than during the northern summer. Note, however, that this
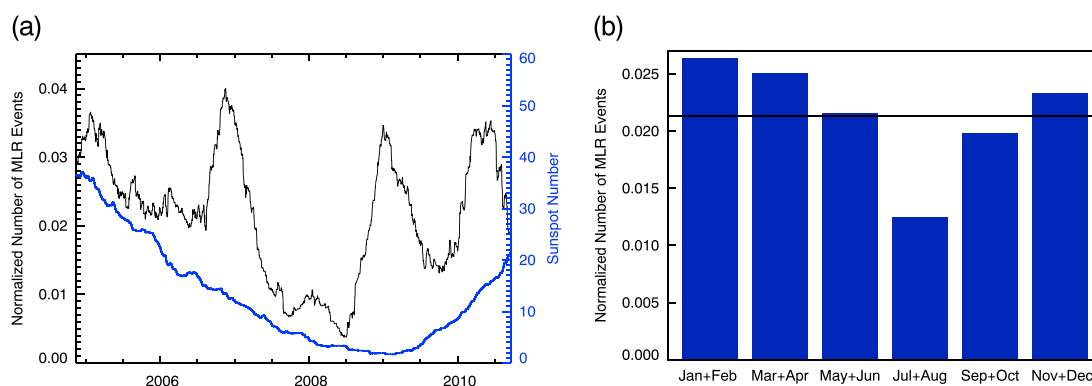
(a)

(b)

Figure 2. (a) Number of MLR events observed by the DEMETER spacecraft in a moving 90 day wide time window normalized by the total number of DEMETER half orbits for which the VLF Survey mode data were available in a given time interval is plotted by the black curve. The blue curve shows the smoothed sunspot number during the analyzed time interval. (b) Monthly variation of the number of identified MLR events normalized by the total number of DEMETER half orbits for which the VLF Survey mode data were available in given months. The overplotted horizontal solid line shows the mean normalized number of identified MLR events.

effect is not observed in all years during our 6.5 year long record (see year 2006). The solid horizontal line overplotted in the figure corresponds to the mean normalized number of detected MLR events (0.021).

Former studies showed that MLR events occur more often during/after the periods of increased geomagnetic activity characterized by the *Kp/Dst* index [*Rodger et al.*, 2000b; *Němec et al.*, 2009]. In the present study we use a superposed epoch method to search for a possible connection between the MLR occurrence, the solar wind parameters (proton density, flow speed, flow pressure, and sign of interplanetary magnetic field (IMF) B_z), the occurrence of interplanetary (IP) shocks in the solar wind, and the geomagnetic indices (*Kp*, *Dst*, and *AE*). The variations of the mean values of these possible control parameters are investigated as a function of the time relative to the times of MLR events. A time interval spanning from 1 week before to 1 week after the event is used. Moreover, a standard deviation of the mean value estimate (which is $\sqrt{1230}$ times smaller than the standard deviation of the whole data set) is calculated at each time.

A connection between the solar wind parameters and the occurrence of MLR events is analyzed in Figure 3 using the superposed epoch analysis. OMNI 1 h time resolution solar wind data time shifted to the bow shock location have been used (http://omniweb.gsfc.nasa.gov). The results obtained for the proton density, flow speed, dynamic pressure, and sign of IMF B_z component are shown in Figures 3a–3d, respectively. The black curves correspond to average values, while the red curves show ± 3 standard deviation contours of these mean value estimates. Figure 3a shows that the mean proton density decreases significantly around the times of MLR events and during the day after them, on average by about 20%. Figure 3b shows that the MLR events generally occur during/shortly after periods of increased solar wind speeds. The mean solar wind speed is about 50 km/s above its average value approximately 1 day before the events, and it gradually decreases afterward. The fluctuations of the average variation of the solar wind dynamic pressure shown in Figure 3c are rather large. However, it can be seen that the MLR events are on average associated with an approximately 20% increase of the dynamic pressure occurring several days before the time of the events. Figure 3d shows that the ratio of positive IMF B_z values (i.e., the number of MLR events for which B_z was positive at a given time over the total number of MLR events) decreases before the time of the events, while there is a sharp increase of this ratio at the time of the events. We have also verified whether the parameters plotted in Figures 3a–3c behave differently for northward or southward IMF, but it does not seem to be the case. We note that although the observed variations of solar wind parameters are statistically significant and clearly identifiable in the plots, the amplitude of the observed effects is rather small as compared to typical fluctuations of the analyzed parameters. This means that the variation of the solar wind parameters for a single MLR event may be significantly different than the average trends depicted in Figure 3.

Figure 4 shows the superposed epoch analysis of the connection between the occurrence of MLR events and IP shocks. The shocks were identified by an automatic procedure of *Kruparova et al.* [2013] and manually verified. Altogether, 282 shocks were identified in the time interval covered by the DEMETER mission (6.5 years). We note that among these, 122 IP shocks were fast forward, 37 IP shocks were fast reverse, 63 IP shocks were slow forward, and 60 IP shocks were slow reverse [*Burlaga*, 1971]. However, the total number of identified IP shocks
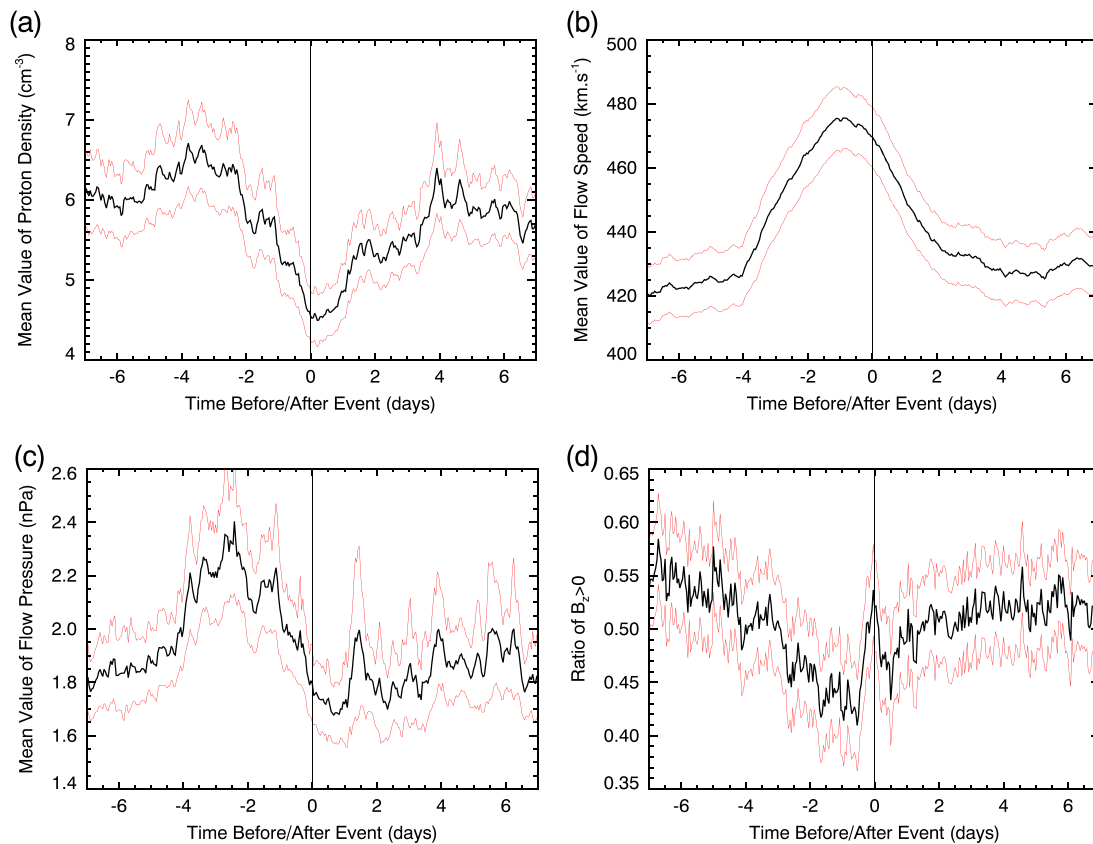
Figure 3. Superposed epoch analysis of the MLR occurrence as a function of selected solar wind parameters. The black curves correspond to mean dependencies, while the red curves correspond to ±3 standard deviations from the mean values. (a) The results obtained for the proton number density. (b) The results obtained for the flow speed. (c) The results obtained for the dynamic pressure. (d) The results obtained for the sign of IMF B_z.

was not high enough to allow us to investigate the effect of each IP shock type independently. For the same reason, we also did not attempt to classify the IP shocks according to their strengths (Mach numbers) and/or shock normal directions.

Mean normalized number of MLR events as a function of the time relative to the times of IP shocks is shown by the black curve in Figure 4. The normalized numbers of MLR events were calculated in a moving 1 day long time interval as the number of MLR events detected during a given time interval divided by the total number of DEMETER half orbits in this interval for which the VLF Survey mode data were available. The red curves correspond to ±3 standard deviations of the mean value estimate. An increase of the mean normalized number of MLR events by about 50% is well noticeable several days after the times of IP shocks. However, the standard deviation estimates indicate that this effect is statistically not so significant as the results from Figure 3, because of low number of IP shocks. Note that we plot the time relative to the times of the shocks in Figure 4 in place of the time relative to the times of the MLR events used in Figure 3. Since the number of identified IP shocks (282) is lower than the number of identified MLR events (1230), we believe that this approach makes more sense than to analyze "mean IP shock occurrence rate" as a function of the time relative to the times of the MLR events (although the two approaches are in fact equivalent and produce comparable results). It should be also noted that the times of the shocks used in the calculation are the times when the shocks were detected by the solar wind monitoring spacecraft, not the times when they are expected to reach the magnetosphere. However, the time difference due to the finite shock speed is on the order of a few hours, i.e., much lower than the time scales considered in Figure 4, and it does not therefore affect the obtained results.

The results of the analysis of Kp, Dst, and AE indices are shown in Figures 5a – 5c, respectively. The format is the same as in Figure 3. It can be seen that the MLR occurrence is statistically related to significant variations of the three geomagnetic indices. Specifically, MLR events occur preferentially about 1 to 2 days after the periods
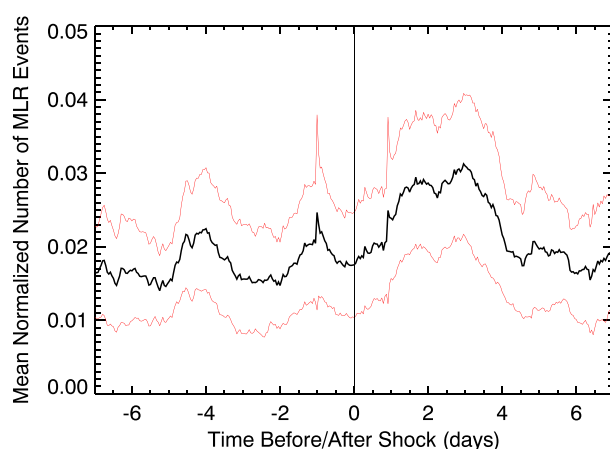
Figure 4. Mean normalized number of MLR events as a function of the time relative to the times of interplanetary shocks is shown by the black curve. The normalized numbers of MLR events were calculated in a moving 12 h long time interval as the number of MLR events detected during a given interval divided by the total number of DEMETER half orbits in this interval for which the VLF Survey mode data were available. The red curves correspond to ± 3 standard deviations from the mean values.

of increased geomagnetic activity (higher *Kp*, lower *Dst*, and higher *AE*). Again, it should be noted that the absolute value of this increase is on average rather small, and it becomes statistically significant only due to the large number of MLR events included in the analysis.

3.2. MLR and Precipitating Electrons

Němec et al. [2009] reported that the number of MLR events occurring over the Atlantic Ocean is lower than the number of events that occur at other geomagnetic longitudes. Specifically, the probability of occurrence of MLR events at geomagnetic longitudes of $0-100°$ was reported to be about half its value at other geomagnetic longitudes. It was suggested that this might be related to the lack of energetic electrons in the drift loss cone above and eastward from the SAA. We use the extended data set of MLR events, along with the DEMETER measurements of energetic electrons close to the drift loss cone, to verify this possibility. We also investigate variations of the measured energetic electron spectra related to MLR events.

The occurrence rate of identified MLR events as a function of the geomagnetic longitude is plotted in Figure 6 by the black curve. The occurrence rate was calculated as the total duration of identified MLR events in a given longitudinal bin divided by the total duration of DEMETER VLF Survey mode data acquired at corresponding geomagnetic longitudes. The upper estimates of the standard deviations of the occurrence rate in individual longitudinal bins are marked. For a given longitudinal bin, the upper estimate of the standard deviation of the occurrence rate was calculated as a standard deviation of the binomial distribution, i.e., $\sqrt{p(1-p)/N}$, where p is the occurrence rate of MLR events in the given longitudinal bin and N is the total number of DEMETER half orbits with VLF Survey mode data available contributing to this bin. Note that this is an upper estimate of the standard deviation, as N should be in principle equal to the number of independent data points contributing to the bin. However, it is not clear how the number of independent data points should be determined. Specifically, the presence/absence of an MLR event in two consecutive closely separated times is obviously highly correlated. We therefore use the total number of DEMETER half orbits with VLF Survey mode data available contributing to the bin as a lower estimate of the number of independent data points, which leads to the upper estimate of the standard deviation of the MLR occurrence rate.

The lower MLR occurrence rate at geomagnetic longitudes between about 0 and 120° can be clearly seen. The red curve in Figure 6 represents the longitudinal dependence of the mean number of counts per second of energetic electrons with energies between 73 keV and 2342 keV detected by the IDP instrument on board the DEMETER spacecraft [*Sauvaud et al.*, 2006]. The detector of the Instrument for the Detection of Particles (IDP) instrument is oriented perpendicularly to the orbital plane of the satellite. Considering that the satellite orbit is almost polar and circular, the pitch angle of the detected particles is close to 90° (the median value is 83.7°, the 0.25 quartile value is 77.1°, and the 0.75 quartile value is 90.4°). Taking into account the low altitude of the DEMETER spacecraft, this corresponds to measurements of energetic electrons inside the drift loss cone or just outside. In the Survey mode, there are 128 energy channels, and the time resolution of the obtained electron energy spectra is 4 s [*Sauvaud et al.*, 2006]. The largest electron fluxes are detected at geomagnetic longitudes between about 0 and 80°, corresponding to the location of the SAA. This longitudinal dependence is the same for principally all electron energies, and we thus do not distinguish according to the electron energy in Figure 6. The MLR occurrence rate has a minimum at these longitudes, and it only increases at geomagnetic longitudes larger than about 120°.
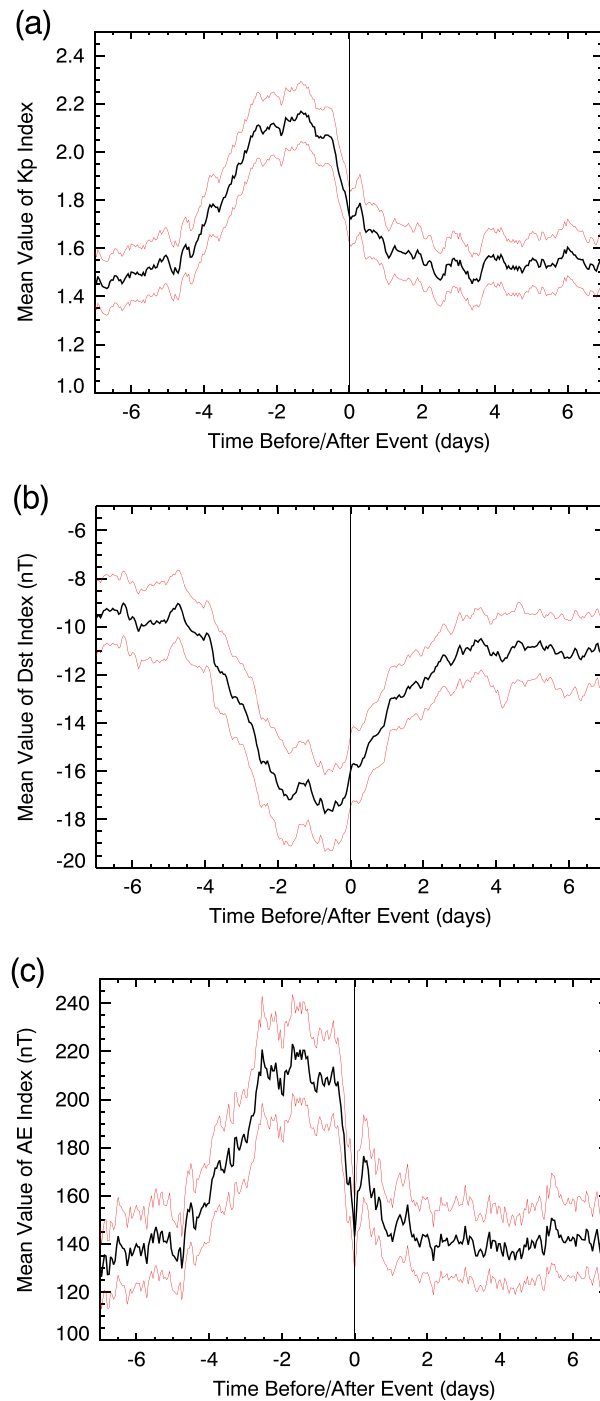
Figure 5. Superposed epoch analysis of MLR occurrence as a function of selected geomagnetic indices. The format is the same as in Figure 3. (a) The results obtained for the *Kp* index. (b) The results obtained for the *Dst* index. (c) The results obtained for the *AE* index.

These results indicate that the MLR occurrence is related to energetic electrons in the drift loss cone. When these electrons precipitate upon reaching the geomagnetic longitudes of the SAA, the MLR occurrence rate significantly decreases. This can be due to two different reasons: (i) electrons in the drift loss cone are directly responsible for the MLR generation, and their lack above/eastward from the SAA thus suppresses the MLR generation and (ii) scattering of energetic electrons into an empty drift loss cone is a damping mechanism for the waves, resulting thus in a lower MLR occurrence.
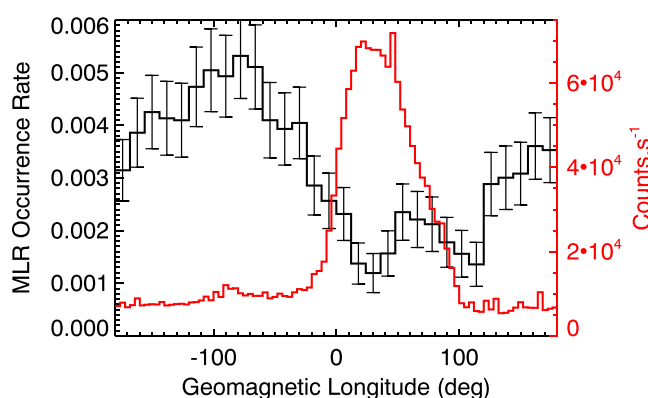
Figure 6. Occurrence rate of MLR events as a function of the geomagnetic longitude is plotted by the black curve using the scale on the left-hand side. The upper estimates of the standard deviations of the occurrence rate in individual longitudinal bins are marked (see text for more details on their calculation). The red curve (scale on the right-hand side) shows the longitudinal dependence of the mean number of counts per second of energetic electrons with energies between 73 keV and 2342 keV detected by the DEMETER spacecraft.

Since Figure 6 shows the longitudinal dependence of the number of counts averaged over all latitudes, it is of interest to determine the geomagnetic latitudes where the main part of the precipitation takes place. Figure 7 shows the longitudinal dependencies of the average number of counts of energetic electrons with energies between 73 keV and 2342 keV detected by the IDP instrument in four different latitudinal ranges of the DEMETER spacecraft. The black curve was obtained for geomagnetic latitudes larger than 0°, the blue curve was obtained for geomagnetic latitudes between −40 and 0°, the green curve was obtained for geomagnetic latitudes between −48 and −40°, and the red curve was obtained for geomagnetic latitudes lower than −48°. No longitudinal variation of the energetic electron flux is seen at geomagnetic latitudes lower than about −48° (red curve) and at geomagnetic latitudes larger than 0° (black curve). This means that the effect of the SAA is limited only to geomagnetic latitudes between about −48 and 0°. Considering the altitude of the DEMETER spacecraft, and taking into account that the MLR occurrence seems to be affected by the presence of the SAA, this suggests that MLR events are generated at L shells lower than about 2.5.

Assuming that the MLR events are generated at the same MLTs as they are observed (i.e., they do not propagate in the azimuthal direction), we can try to monitor variations in the electron distribution related to the MLR occurrence. Given the limitations of the IDP instrument on board DEMETER, this analysis concerns only electrons inside the drift loss cone or just outside, with no further distinction according to their pitch angles.
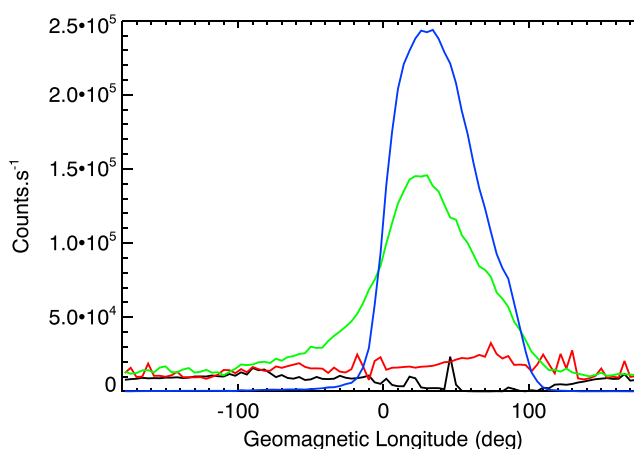

Figure 7. Longitudinal dependence of the mean number of counts of energetic electrons with energies between 73 keV and 2342 keV in four different latitudinal ranges. The black curve was obtained for geomagnetic latitudes larger than 0°, the blue curve was obtained for geomagnetic latitudes between −40 and 0°, the green curve was obtained for geomagnetic latitudes between −48 and −40°, and the red curve was obtained for geomagnetic latitudes lower than −48°.
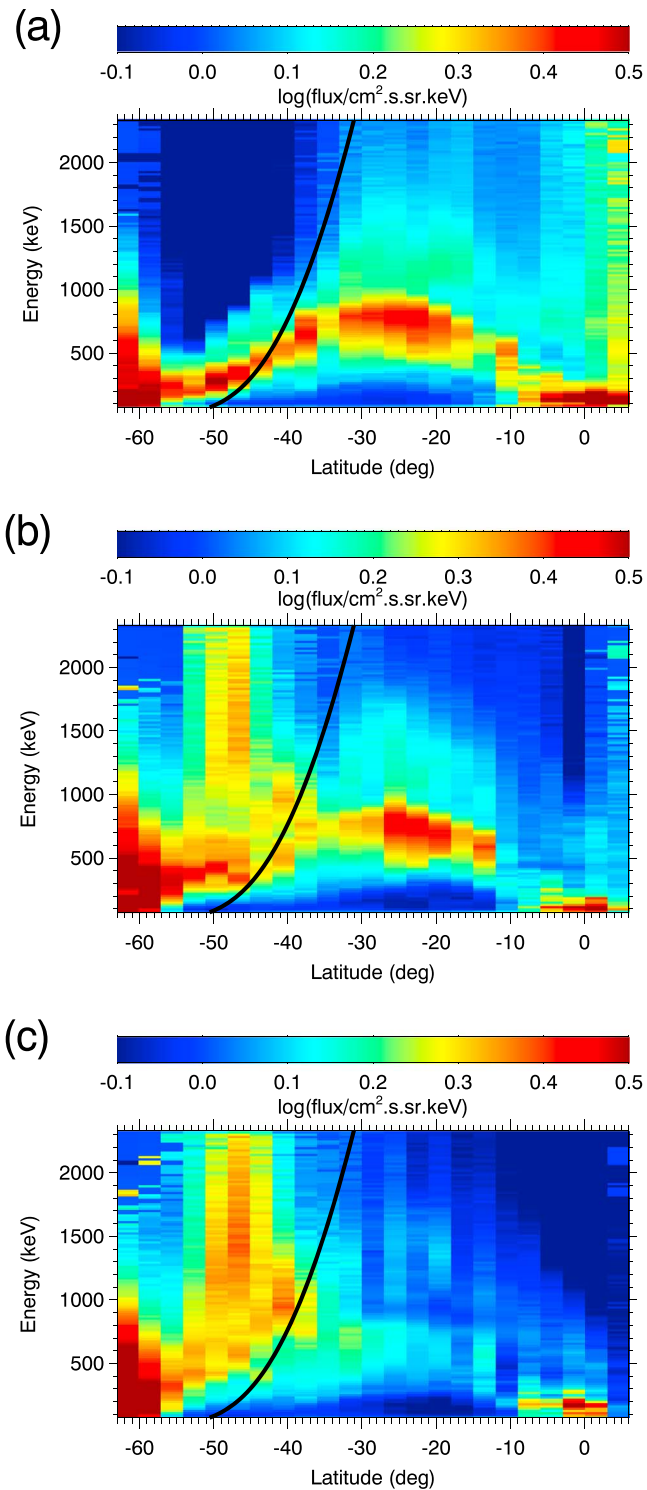
Figure 8. Variations of the energetic electron flux detected by the DEMETER spacecraft at geomagnetic longitudes corresponding to the SAA (0–80°) in relation to MLR events as a function of the electron energy and the geomagnetic latitude. The difference of median electron fluxes measured during spacecraft orbits related to MLR events and median electron fluxes measured during the whole duration of the mission is plotted. (a–c) Orbits preceding MLR events, containing MLR events, and following MLR events, respectively. The black curves correspond to calculated resonant energies (see text).

If an MLR event is observed during a half orbit slightly westward from the SAA, the electrons in the drift loss cone which have interacted with it (which drift eastward) should precipitate and be detected during a neighboring half orbit at the geomagnetic longitudes of the SAA. If an MLR event is observed during a half orbit slightly eastward from the SAA, then the electrons detected above the SAA should be characteristic of an electron population able to trigger MLR events but not yet influenced by MLR. We note that this intrinsically assumes that the electron distribution related to the MLR occurrence does not change significantly on time scales comparable to the time separation between consecutive DEMETER orbits (about 1.7 h). Also, the half orbits used for the analysis of precipitating electrons, which precede/follow the half orbits with MLR events, typically do not contain MLR events [*Němec et al.*, 2009].

Variations of the energetic electron flux detected by the IDP instrument at the geomagnetic longitudes corresponding to the SAA (0–80°) in relation to MLR events are analyzed in Figure 8. The difference between the median electron fluxes related to the presence of MLR events and the median electron fluxes measured during the whole duration of the DEMETER mission is color coded as a function of the electron energy and the geomagnetic latitude. Due to the Earth's rotation, the spacecraft effectively moves westward. The condition of a half orbit being immediately followed by a half orbit with an MLR event is therefore equivalent to an MLR event observed westward. Then Figures 8a–8c show the difference obtained for electron fluxes measured during spacecraft orbits preceding MLR events, containing MLR events, and following MLR events, respectively. Figure 8c corresponds to the situation of an MLR event observed eastward. The results are not plotted for geomagnetic latitudes larger than 6°, as the energetic electron fluxes in this region are generally too low to be detected.

One can see an increase of energetic electron fluxes at geomagnetic latitudes of about −60° (corresponding to the edge of the outer radiation belt) and energies up to about 1000 keV in Figures 8a–8c. As the increase is about the same in all panels, it does not seem to be related to MLR but it is rather a result of the increased geomagnetic activity at the times of MLR occurrence. Variations of energetic electron flux which are different in each panel—and which are thus possibly related to MLR—are seen at geomagnetic latitudes between about −55 and −15°. The fluxes of energetic electrons which possibly interacted with MLR (Figure 8a) are significantly suppressed at geomagnetic latitudes of about −55° and at energies larger than 500 keV as compared to the fluxes of energetic electrons which will possibly interact with MLR (Figure 8c). On the other hand, the fluxes of energetic electrons which possibly interacted with MLR are enhanced at lower energies. This increase occurs in the energy band which varies smoothly with geomagnetic latitude, peaking at geomagnetic latitudes of about −30°. The fluxes of energetic electrons which are possibly interacting with MLR (Figure 8b) are in between of those seen in Figures 8a and 8c, as one might expect.

In this regard it may be instructive to estimate resonant energies of electrons which may interact with MLR. We consider the first-order cyclotron resonance for relativistic electrons [e.g., *Koons et al.*, 1991]. We assume that the interaction occurs in the equatorial plane and that the wave vector is field aligned there. We use the dipole magnetic field model and the plasmasphere density model of *Denton et al.* [2004]. It is then possible to calculate a resonant energy for a given wave frequency and a given L shell. We select 3 kHz as a typical frequency of the MLR events [*Němec et al.*, 2009]. The black curves in Figures 8a–8c represent the resulting resonant energies. The resonant energy at $L = 2.5$ (corresponding to the geomagnetic latitude $\lambda_m \approx 48°$ at DEMETER altitudes) is about 130 keV, at $L = 2$ (corresponding to $\lambda_m \approx 42°$) about 535 keV, and at $L = 1.5$ (corresponding to $\lambda_m \approx 31°$) about 2330 keV.

3.3. Locations of MLR Events

The blue points in Figure 9 show the minimum L value of individual MLR events as a function of the model plasmapause location (L_{pp}) of *Carpenter and Anderson* [1992]. The median of dependence is overplotted by the blue line. The red points show the maximum L value of individual MLR events as a function of the model plasmapause location, and the corresponding median dependence is overplotted by the red line. The black diagonal line corresponds to the one to one dependence. It divides the graph into two parts: inside the plasmasphere (bottom right) and outside the plasmasphere (top left). Some MLR events appear to extend well beyond the plasmasphere, while some of them are limited inside the plasmasphere. The L shells of DEMETER observations were determined by tracing the magnetic field lines using the International Geomagnetic Reference Field (IGRF) and Tsyganenko 89 [*Tsyganenko*, 1989] magnetic field models to the point where the radial component of the magnetic field reverses sign. However, the results obtained using a magnetic dipole are globally nearly the same. One should be aware that the L shell at large geomagnetic latitudes changes
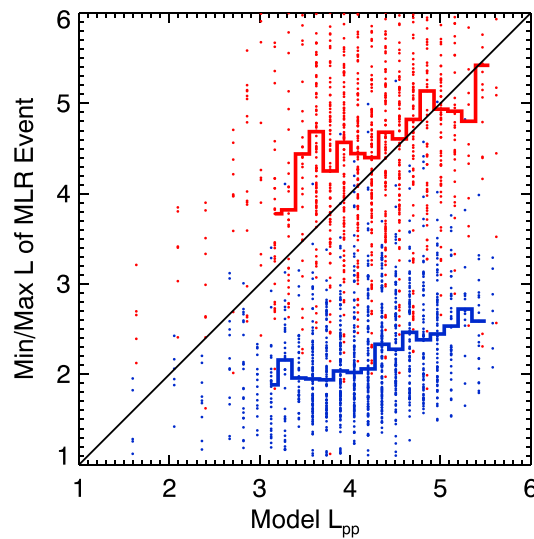
Figure 9. The blue points show the minimum *L* value of individual MLR events as a function of the model plasmapause location. The red points show the maximum *L* value of individual MLR events as a function of the model plasmapause location. The overplotted blue and red curves correspond to respective median dependencies. The black diagonal line divides the graph into two parts—(bottom right) inside the plasmasphere and (top left) outside the plasmasphere.

rapidly with the spacecraft position, which may result in significant inaccuracies of the maximum L shells of MLR events. Moreover, one should consider the inaccuracies due to the location of the plasmapause being determined using a simple empirical model. Nevertheless, the median dependence indicates that the maximum L shell of MLR events approximately follows the plasmapause location. Moreover, it can be seen that the minimum L shells of MLR events are also positively correlated with L_{pp}.

3.4. Detailed Wave Analysis

Multicomponent measurements obtained by the DEMETER satellite during the Burst mode in the extra low frequency (ELF) range allow us to perform a detailed analysis of the wave propagation [*Santolík et al.*, 2006a]. However, the Nyquist frequency limit of the ELF range is only 1.25 kHz, while most of the MLR events are observed at frequencies between about 2 and 6 kHz [*Němec et al.*, 2009]. Consequently, only two MLR events from our list of 1230 events are suitable for the detailed wave analysis. These are shown in Figures 10 and 11. Figures 10a and 11a show the frequency-time spectrograms of

power spectral density of electric field fluctuations and the frequency-time spectrograms of power spectral density of magnetic field fluctuations, top to bottom, respectively. The influence of antialiasing filters close to the Nyquist frequency is taken into account by careful amplitude and phase calibration of the measured
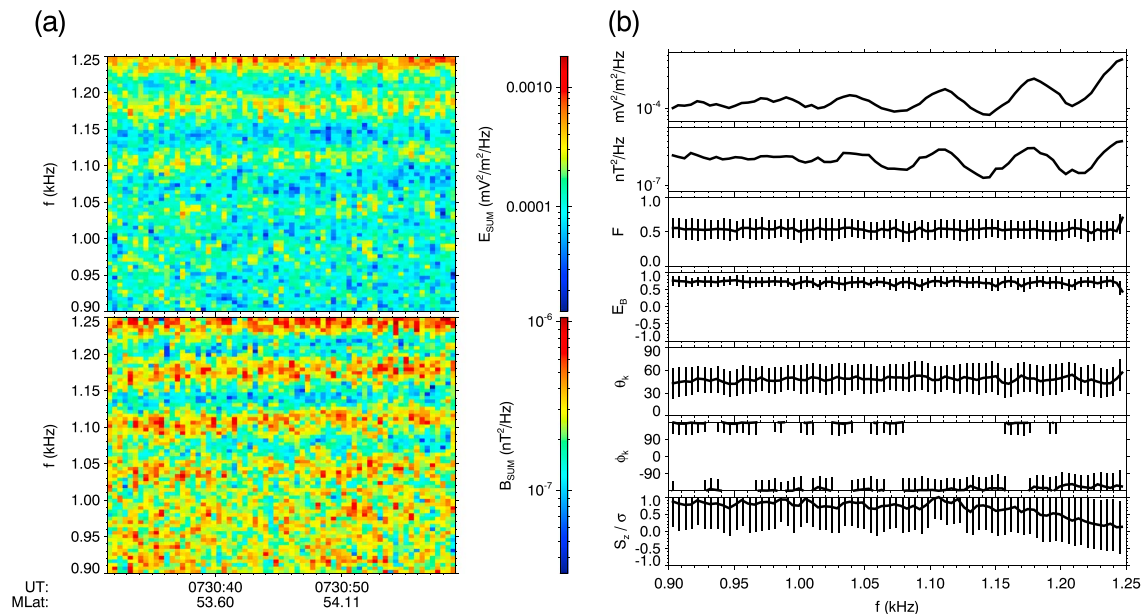

Figure 10. Detailed wave analysis of an MLR event observed on 15 September 2005 around 07:30 UT. (a) Frequency-time spectrograms of power spectral densities of electric and magnetic field fluctuations. (b) (first panel) Frequency spectrum of electric field fluctuations, (second panel) frequency spectrum of magnetic field fluctuations, (third panel) frequency dependence of the planarity of magnetic field fluctuations, (fourth panel) frequency dependence of the ellipticity of magnetic field fluctuations, (fifth panel) frequency dependence of the polar angle of the wave vector direction, (sixth panel) frequency dependence of the azimuthal angle of the wave vector direction, and (seventh panel) frequency dependence of the component of the Poynting flux along the ambient magnetic field normalized by the standard deviation (see text of the paper for a more detailed description of all the parameters). The thin vertical lines mark the standard deviations.
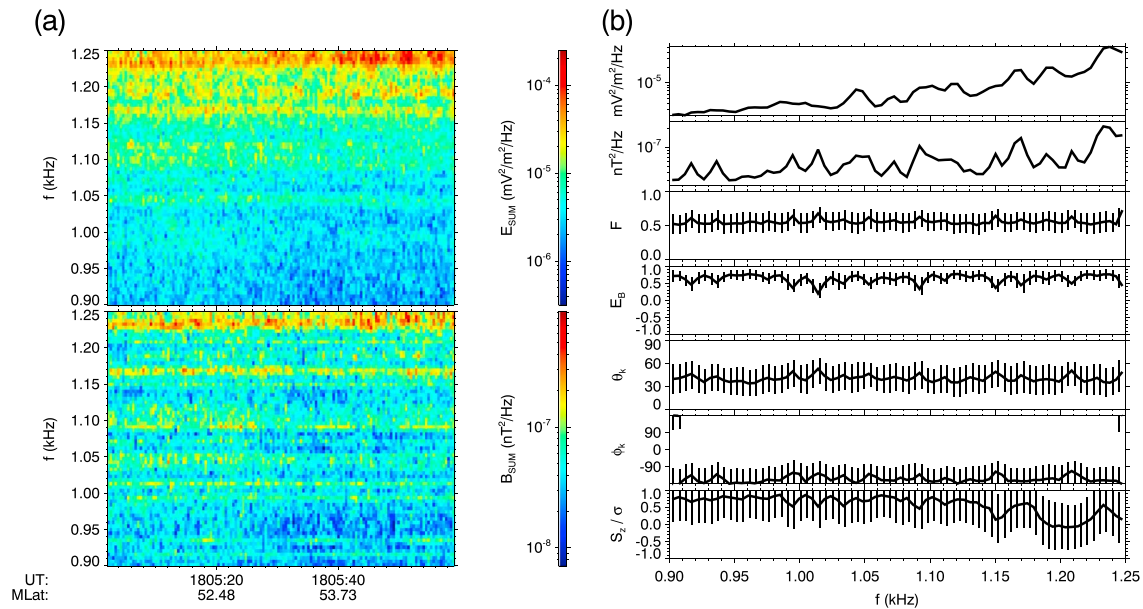
Figure 11. The same as Figure 10 but for the MLR event observed on 13 May 2006 around 18:05 UT.

data. Figures 10b and 11b contain the appropriate frequency spectra and the results of the wave analysis as a function of the frequency. The thin vertical lines mark the standard deviations of individual parameters, calculated from the values obtained at individual times. Figures 10b and 11b (first and second panels) correspond to the frequency spectra of electric and magnetic field fluctuations, respectively. The peaks at frequencies corresponding to individual MLR lines can be clearly seen in Figure 10, but they are somewhat obscured in Figure 11 due to the interferences. Both events were observed in the Northern Hemisphere, at geomagnetic latitudes of about 50–55°. The obtained values of wave propagation parameters are about the same for both events.

Figures 10b and 11b (third panel) show the frequency dependence of the planarity of magnetic field fluctuations [*Santolík et al.*, 2003]. The values are slightly larger than 0.5, indicating that the assumption of a single plane wave is roughly applicable but not entirely fulfilled. Figures 10b and 11b (fourth panel) show the ellipticity of magnetic field fluctuations, defined as the ratio of minor to major axes of the polarization ellipse. Moreover, a sign is added to express the sense of polarization. Negative values of the ellipticity correspond to left-handed polarized waves, while positive values of the ellipticity correspond to right-handed polarized waves. The observed values of ellipticity are close to 1, meaning that the MLR events are right-handed and nearly circularly polarized.

Figures 10b and 11b (fifth and sixth panels) show the polar and azimuthal angles of the wave vector direction calculated from the magnetic parts of the spectral matrices [*Santolík et al.*, 2003]. The values of the polar angles are close to 45°, corresponding to oblique wave propagation. The azimuthal angles of the wave vector direction are close to ±180°, corresponding to the wave propagation toward lower L shells. It should be noted that the usage of solely magnetic field data leaves an ambiguity of ±180° when determining the wave vector direction. This is resolved using the electric field data, which allows us to select the proper direction. We determine the component of the Poynting flux along the ambient magnetic field normalized by the standard deviation. The obtained results are depicted in Figures 10b and 11b (seventh panel). The observed positive values correspond to the parallel component of the Poynting vector oriented along the ambient magnetic field. The results of the wave propagation analysis therefore indicate that the emissions propagate from larger radial distances and larger geomagnetic latitudes.

4. Discussion

The large set of MLR events observed during the whole DEMETER mission, i.e., during about 6.5 years, is sufficient to verify a possible influence of the solar activity on the MLR occurrence. The results depicted in Figure 2a

suggest that the number of MLR events can sometimes be larger for a larger solar activity. This might be explainable in terms of enhanced solar wind driving. However, the overall correlation is not convincing, and other effects probably also play a role. The seasonal dependence of the MLR occurrence analyzed in Figure 2b shows that the events can occur more often during the northern winter and spring than during the northern summer. This can be contrasted with the results of *Rodger et al.* [2000b], who reported quite an opposite dependence based on the analysis of data from the Halley station, Antarctica. However, they reported that the proportion of MLR events present as a part of the overall wave activity is roughly constant throughout the year. The seasonal dependence of the overall wave activity observed by the DEMETER spacecraft was analyzed by *Němec et al.* [2010b]. Although they focused primarily on the analysis of the wave activity above lightning regions, it can be seen in their Figures 2 and 3 that the median wave intensity at higher latitudes is larger during the northern winter than during the northern summer. This might be possibly related to the lower overall lightning activity during the northern winter [*Christian et al.*, 2003] and therefore lower lightning-induced electron precipitation [*Gemelos et al.*, 2009]. The lower lightning-induced electron precipitation may result in more electrons in the drift loss cone, which possibly enhances the wave generation/suppresses the wave attenuation, as is suggested by Figure 6.

Superposed epoch analyses allowed us to identify most favorable geomagnetic conditions and solar wind parameters for MLR events to occur. The results concerning the Kp and Dst indices depicted in Figures 5a and 5b are consistent with the results obtained using a smaller data set by *Němec et al.* [2009]. The respective differences in the mean values of the indices (lower values of mean Kp index and larger values of mean Dst index in the present study) can be attributed to the fact that the newly added data were obtained primarily during the solar minimum. A surprising effect is the sudden sharp increase of the ratio of positive IMF B_z values at the time of MLR events in Figure 3d. This indicates that although the events are related to the periods of enhanced geomagnetic activity, they typically occur just when it is about to finish. It is noteworthy that a corresponding trend can be seen in the results obtained for the AE index in Figure 5c, where the mean value of the AE index suddenly drops at the time of the events. These results are consistent with MLR events being a recovery phase phenomenon. Although MLR events occur more often after the IP shock passage, this relationship is clearly not one to one. There are MLR events for which no corresponding IP shock was identified, and there are IP shocks which are not followed by MLR events.

As demonstrated in Figure 8, the observed electron flux at energies up to about 1000 keV is significantly enhanced around the times of MLR events at geomagnetic longitudes of the SAA and geomagnetic latitudes of about −60°. However, the particles at these high L shells are nearly unaffected by the presence of the SAA. This suggests that the flux increase is not related to the MLR generation, but it is rather a result of the increased geomagnetic activity around the times of MLR events. This conclusion is also consistent with the increase being about the same in all panels of Figure 8, i.e., independent of the azimuthal separation between detected electrons and MLR events.

Important variations of the energetic electron flux thus seem to be at lower latitudes. The calculated resonant energies at L shells corresponding to DEMETER geomagnetic latitudes between about −48 and −42° ($L \approx 2-2.5$) roughly correspond to the energy range where the energetic electron flux is enhanced in Figure 8a, but they increase much faster at lower L shells. These experimental results are indicative of electrons possibly playing a role in the MLR generation. However, it is difficult to distinguish the electron population responsible for the MLR generation from the electron population which is only affected by the already-generated MLR events using the available data. Further experimental and, most importantly, theoretical studies are needed to understand how the MLR events are generated.

Figure 9 shows that the median value of the maximum L shell of the observed MLR events is correlated with the model plasmapause location. The large scatter of the data points can be partly attributed to the inaccuracy of the plasmapause model location, but it is clear that MLR events may also leak out of the plasmasphere. For low model L_{pp} values the MLR events seem to span more often outside of the plasmasphere. On the other hand, for large model L_{pp} values the MLR events are more often confined inside the plasmasphere. We believe that this might indicate the importance of the plasmapause ducting [e.g., *Inan and Bell*, 1977] for the propagation of at least some MLR events from their source region down to the altitudes of the DEMETER spacecraft. This plasmapause ducting, along with the deviation of the guided waves toward lower geomagnetic latitudes at altitudes of several thousands of kilometers [*Inan and Bell*, 1977], is consistent with the positive correlation between the minimum L values of MLR events and L_{pp}. It would be also consistent with the results of

a detailed wave analysis, which shows that the emissions propagate unducted, and they come from larger radial distances and larger geomagnetic latitudes.

Similar propagation pattern was observed for ELF hiss emissions by *Santolík and Parrot* [1999, 2000] using the data from the low-orbiting Freja spacecraft. Both plane wave approximation and wave distribution function showed that the downgoing right-hand polarized emissions propagated with an equatorward component at geomagnetic latitudes below 65°. A ray-tracing study by *Santolík et al.* [2006b] indicated that sources of these waves might be found in the equatorial region outside the plasmapause. These propagation properties are also similar to the propagation properties derived recently for quasiperiodic emissions [*Němec et al.*, 2013a, 2013b]. The observed large L shell extent of MLR events [*Parrot et al.*, 2007; *Němec et al.*, 2012b] could thus be purely a propagation effect, as even a spatially limited source region can influence a large volume of space [*Němec et al.*, 2014].

Finally, it is noteworthy that the results of a statistical investigation of quasiperiodic emissions measured by the DEMETER spacecraft [*Hayosh et al.*, 2014] indicate that MLR events and quasiperiodic emissions have more in common than only the similar propagation properties. Namely, both types of emissions typically occur after the periods of higher geomagnetic activity, they occur less frequently at the geomagnetic longitudes of the SAA, and they are both primarily dayside phenomena. In fact, one could possibly think of MLR events as the frequency modulation of hiss-like emissions and of quasiperiodic events as the time modulation of hiss-like emissions. However, a detailed investigation of a possible relation between these phenomena is beyond the scope of the present paper, and it will be done in the future.

5. Conclusions

A list of all MLR events identified in the DEMETER data set has been compiled for the entire duration of the mission (2004–2010). Altogether, this list contains 1230 MLR events, which probably represents the largest MLR data set available to date. We have demonstrated a possible seasonal dependence of the MLR occurrence. MLR events are often (but not always) more frequent during the northern winter and spring than during the northern summer. We have shown the statistical relation between the MLR occurrence, solar wind parameters, and geomagnetic indices. The MLR occurrence was shown to be lower at geomagnetic longitudes between about 0 and 120°, corresponding to the area of the SAA. This indicates that MLR events interact with energetic electrons in the drift loss cone, which precipitate upon reaching the geomagnetic longitudes of the SAA. Energetic electron fluxes observed at the times of MLR events were compared with the long-term distribution. The resulting energy-latitudinal plots of electron flux variations might be indicative of electrons playing a role in the MLR generation. Finally, we have performed a detailed wave analysis of two MLR events for which high-resolution multicomponent data were available. We have shown that the waves are right-handed and nearly circularly polarized, propagating at oblique wave normal angles from larger geomagnetic latitudes and larger L shells.

References

Bell, T. F., J. P. Luette, and U. S. Inan (1982), ISEE 1 observations of VLF line radiation in the Earth's magnetosphere, *J. Geophys. Res.*, *87*(A5), 3530–3536.

Berthelier, J. J., et al. (2006), ICE, the electric field experiment on DEMETER, *Planet. Space Sci.*, *54*, 456–471.

Bullough, K. (1995), Handbook of atmospheric electrodynamics, in *Power Line Harmonic Radiation: Sources and Environmental Effects*, vol. 2, edited by H. Volland, pp. 291–332, CRC Press, Boca Ralton, Fla.

Burlaga, L. F. (1971), Hydromagnetic waves and discontinuities in the solar wind, *Space Sci. Rev.*, *12*, 600–657.

Carpenter, D. L., and R. R. Anderson (1992), An ISEE/Whistler model of equatorial electron density in the magnetosphere, *J. Geophys. Res.*, *97*(A2), 1097–1108.

Christian, H. J., et al. (2003), Global frequency and distribution of lightning as observed from space by the optical transient detector, *J. Geophys. Res.*, *108*(D1), 4005, doi:10.1029/2002JD002347.

Denton, R. E., J. D. Menietti, J. Goldstein, S. L. Young, and R. R. Anderson (2004), Electron density in the magnetosphere, *J. Geophys. Res.*, *109*, A09215, doi:10.1029/2003JA010245.

Gemelos, E. S., U. S. Inan, M. Walt, M. Parrot, and J. A. Sauvaud (2009), Seasonal dependence of energetic electron precipitation: Evidence for a global role of lightning, *Geophys. Res. Lett.*, *36*, L21107, doi:10.1029/2009GL040396.

Hayosh, M., F. Němec, O. Santolík, and M. Parrot (2014), Statistical investigation of VLF quasiperiodic emissions measured by the DEMETER spacecraft, *J. Geophys. Res. Space Physics*, *119*, 8063–8072, doi:10.1002/2013JA019731.

Inan, U. S., and T. F. Bell (1977), The plasmapause as a VLF wave guide, *J. Geophys. Res.*, *82*(19), 2819–2827.

Koons, H. C., B. C. Edgar, and A. L. Vampola (1991), Precipitation of inner zone electrons by whistler mode waves from the VLF transmitters UMS and NWC, *J. Geophys. Res.*, *86*(A2), 640–648.

Kruparova, O., M. Maksimovic, J. Šafránková, Z. Němeček, O. Santolík, and V. Krupar (2013), Automated interplanetary shock detection and its application to Wind observations, *J. Geophys. Res. Space Physics*, *118*, 4793–4803, doi:10.1002/jgra.50468.

Manninen, J. (2005), Magnetospheric line radiation, in *Some Aspects of ELF-VLF Emissions in Geophysical Research, Sodankylä Geophys. Obs. Publ.*, vol. 98, edited by J. Kultima, pp. 85–110, Oulu Univ. Press, Sodankylä, Finland.

Němec, F., O. Santolík, M. Parrot, and J. J. Berthelier (2006), Power line harmonic radiation (PLHR) observed by the DEMETER spacecraft, *J. Geophys. Res.*, *111*, A04308, doi:10.1029/2005JA011480.

Němec, F., O. Santolík, M. Parrot, and J. J. Berthelier (2007a), Comparison of magnetospheric line radiation and power line harmonic radiation: A systematic survey using the DEMETER spacecraft, *J. Geophys. Res.*, *112*, A04301, doi:10.1029/2006JA012134.

Němec, F., O. Santolík, M. Parrot, and J. J. Berthelier (2007b), Power line harmonic radiation: A systematic study using DEMETER spacecraft, *Adv. Space Res.*, *40*, 398–403.

Němec, F., O. Santolík, M. Parrot, and J. Bortnik (2008), Power line harmonic radiation observed by satellite: Properties and propagation through the ionosphere, *J. Geophys. Res.*, *113*, A08317, doi:10.1029/2008JA013184.

Němec, F., M. Parrot, O. Santolík, C. J. Rodger, M. J. Rycroft, M. Hayosh, D. Shklyar, and A. Demekhov (2009), Survey of magnetospheric line radiation events observed by the DEMETER spacecraft, *J. Geophys. Res.*, *114*, A05203, doi:10.1029/2008JA014016.

Němec, F., M. Parrot, and O. Santolík (2010a), Influence of power line harmonic radiation on the VLF wave activity in the upper ionosphere: Is it capable to trigger new emissions?, *J. Geophys. Res.*, *115*, A11301, doi:10.1029/2010JA015718.

Němec, F., O. Santolík, M. Parrot, and C. J. Rodger (2010b), Relationship between median intensities of electromagnetic emissions in the VLF range and lightning activity, *J. Geophys. Res.*, *115*, A08315, doi:10.1029/2010JA015296.

Němec, F., M. Parrot, and O. Santolík (2012a), Detailed properties of magnetospheric line radiation events observed by the DEMETER spacecraft, *J. Geophys. Res.*, *117*, A05210, doi:10.1029/2012JA017517.

Němec, F., O. Santolík, M. Parrot, and J. S. Pickett (2012b), Magnetospheric line radiation event observed simultaneously on board Cluster 1, Cluster 2 and DEMETER spacecraft, *Geophys. Res. Lett.*, *39*, L18103, doi:10.1012/GL053132.

Němec, F., O. Santolík, M. Parrot, J. S. Pickett, M. Hayosh, and N. Cornilleau-Wehrlin (2013a), Conjugate observations of quasi-periodic emissions by Cluster and DEMETER spacecraft, *J. Geophys. Res. Space Physics*, *118*, 198–208, doi:10.1029/2012JA018380.

Němec, F., O. Santolík, J. S. Pickett, M. Parrot, and N. Cornilleau-Wehrlin (2013b), Quasiperiodic emissions observed by the Cluster spacecraft and their association with ULF magnetic pulsations, *J. Geophys. Res. Space Physics*, *118*, 4210–4220, doi:10.1002/jgra.50406.

Němec, F., J. S. Pickett, and O. Santolík (2014), Multi-spacecraft Cluster observations of quasi-periodic emissions close to the geomagnetic equator, *J. Geophys. Res. Space Physics*, *119*, 9101–9112, doi:10.1002/2014JA020321.

Parrot, M. (Ed.) (2006), *First Results of the DEMETER Micro-Satellite*, vol. 54, pp. 411–558, Elsevier, Amsterdam.

Parrot, M., F. Němec, O. Santolík, and J. J. Berthelier (2005), ELF magnetospheric lines observed by DEMETER, *Ann. Geophys.*, *23*, 3301–3311.

Parrot, M., J. Manninen, O. Santolik, F. Nemec, T. Turunen, T. Raita, and E. Macusova (2007), Simultaneous observation on board a satellite and on the ground of large-scale magnetospheric line radiation, *Geophys. Res. Lett.*, *34*, L19102, doi:10.1029/2007GL030630.

Rodger, C. J., N. R. Thomson, and R. L. Dowden (1995), VLF line radiation observed by satellite, *J. Geophys. Res.*, *100*(A4), 5681–5689.

Rodger, C. J., M. A. Clilverd, K. H. Yearby, and A. J. Smith (1999), Magnetospheric line radiation observations at Halley, Antarctica, *J. Geophys. Res.*, *104*(A8), 17,441–17,447.

Rodger, C. J., M. A. Clilverd, K. Yearby, and A. J. Smith (2000a), Is magnetospheric line radiation man-made?, *J. Geophys. Res.*, *105*, 15,981–15,990.

Rodger, C. J., M. A. Clilverd, K. H. Yearby, and A. J. Smith (2000b), Temporal properties of magnetospheric line radiation, *J. Geophys. Res.*, *105*(A1), 329–336.

Santolík, O., and M. Parrot (1999), Case studies on the wave propagation and polarization of ELF emissions observed by Freja around the local proton gyrofrequency, *J. Geophys. Res.*, *104*(A2), 2459–2475.

Santolík, O., and M. Parrot (2000), Application of wave distribution function methods to an ELF hiss event at high latitudes, *J. Geophys. Res.*, *105*(A8), 18,885–18,894.

Santolík, O., M. Parrot, and F. Lefeuvre (2003), Singuar value decomposition methods for wave propagation analysis, *Radio Sci.*, *38*(1), 1010, doi:10.1029/2000RS002523.

Santolík, O., F. Němec, M. Parrot, D. Lagoutte, L. Madrias, and J. J. Berthelier (2006a), Analysis methods for multi-component wave measurements on board the DEMETER spacecraft, *Planet. Space Sci.*, *54*, 512–527.

Santolík, O., J. Chum, M. Parrot, D. A. Gurnett, J. S. Pickett, and N. Cornilleau-Wehrlin (2006b), Propagation of whistler mode chorus to low altitudes: Spacecraft observations of structured ELF hiss, *J. Geophys. Res.*, *111*, A10208, doi:10.1029/2005JA011462.

Sauvaud, J. A., T. Moreau, R. Maggiolo, J.-P. Treilhou, C. Jacquey, A. Cors, J. Coutelier, J. Rouzaud, E. Penou, and M. Gangloff (2006), High-energy electron detection onboard DEMETER: The IDP spectrometer, description and first results on the inner belt, *Planet. Space Sci.*, *54*, 502–511.

Tsyganenko, N. A. (1989), A magnetospheric magnetic field model with a warped tail current sheet, *Planet. Space Sci.*, *37*(1), 5–20.